UACJ Technical Reports, Vol.12 (2025), pp. 10-16

Paper

Numerical Analysis of Channel-Type Segregations in DC Casting Aluminum Slab*

Keisuke Kamiya** and Takuya Yamamoto***

In the direct chill casting of aluminum alloys, the stripe-shaped segregation called channel-type segregations are formed in the slab, but the mechanism of their formation is not clear, and the casting conditions under which the segregation is minimized have not been found. In this study, it is reported that a numerical simulation model for the Mg segregation have been developed, and the segregation distribution in the Al-Mg alloy slab was numerically analyzed. As a result, the numerical analysis captured Mg segregation similar to that observed in actual slabs. This simulation results showed that the channel-type segregations could be suppressed by colliding the strong down flow with the solidification front.

Keywords: *DC casting, segregation, numerical analysis*

1. Introduction

In the semi-continuous casting process called direct chilled (DC) casting of aluminum alloys, the segregation of solute concentration occurs in the slab. Negative segregation is observed in the center region of the slab, and stripe-shaped segregation, called channel-type segregation is observed around the center region of the slab (**Fig. 1**). Since these segregations cause the changes in the mechanical and chemical properties of the final product, their formation must be suppressed. However, their formation mechanism remains unclear up to now.

In response to such problems, the formation mechanism of channel-type segregation has been attempted to be clarified through numerical simulation by authors[1]. **Fig. 2** shows the numerical results of solute concentration in a DC casting aluminum billet. Although channel-type segregation has been numerically simulated in steel slabs[2], no study has simulated this phenomenon in aluminum alloy DC casting until now; Fig. 2 is the first example reported worldwide. This simulation results allow us to explain in detail how the channel-type segregation is formed during the casting process.

Fig. 3 shows the time evolution of the Mg concentration distribution ahead of the solidification front in DC casting billet[1]. First, as the molten metal solidifies, a zone with high concentration of Mg (a in Fig. 3) is created at the solidification front, and the concentration of Mg causes occurrence of the upward solutal buoyancy flow along solidification front (b) resulting in the solidification delay (c). As a result, Mg is transferred from the low concentration zone toward the high concentration zone of delayed solidification due to Mg partition (d) between the solid and liquid phases. In this way, the low concentration zones (e) are formed below the high concentration zones. This segregation cycle is repeated, resulting in the formation of channel-type segregation.

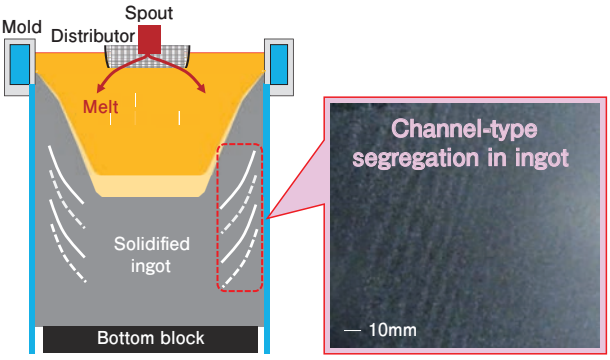

Fig. 1 Schematic view of DC casting and observed segregation on etched slab sample.

* The main part of this paper has been published in Light Metals, (2023), 989-996.

** Process Research Department, Research & Development Center, Marketing & Technology Division, UACJ Corporation.

*** Osaka Metropolitan University, Department of Chemical Engineering, Associate Professor, Ph.D. (Eng.)

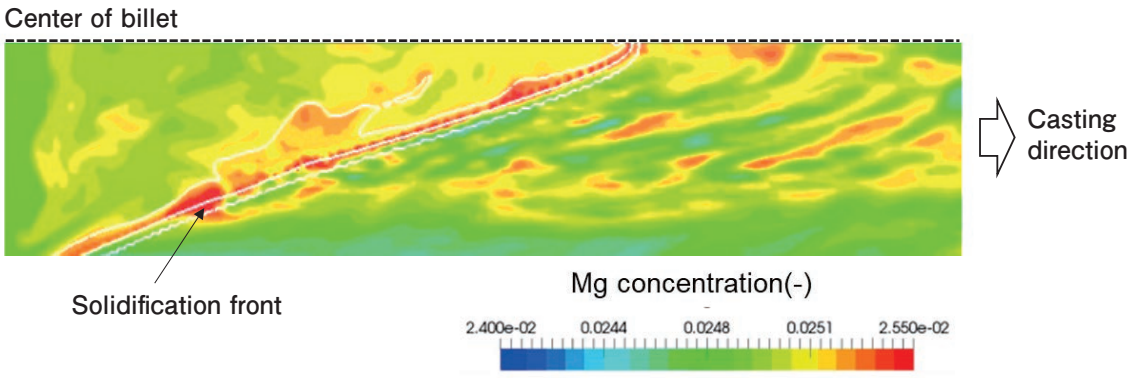

Fig. 2 Numerical analysis result of Al-2.5mass% Mg billet[1].

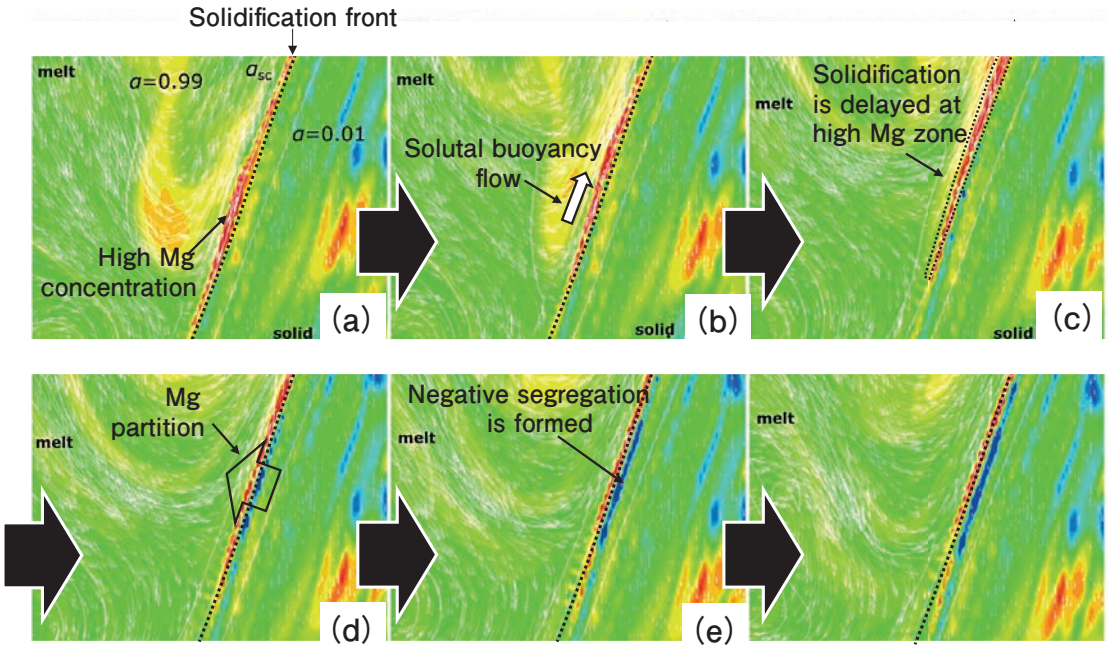

Fig. 3 Formation process of channel-type segregation shown by numerical analysis[1].

As described, the mechanism of channel-type segregation has been cleared, however casting conditions to suppress its occurrence have not yet been found. Therefore, the aim in this paper is to find a casting conditions to suppress the channel-type segregation in DC casting slab of aluminum alloys by the numerical simulation.

2. Numerical simulation method

The numerical simulation model is based on the model proposed by Vreeman et al.[3], and the modified model by Fezi et al.[4], which basically consists of four basic governing equations for the balance of momentum, mass, enthalpy and chemical species concentration with solidification.

Each equation is given as

$$\frac{\partial(\rho \boldsymbol{u})}{\partial t}+\nabla(\rho \boldsymbol{u}\boldsymbol{u})=-\nabla p+\nabla\cdot\left(\frac{\mu_{\mathrm{l}}}{\rho_{\mathrm{l}}}\nabla \boldsymbol{u}\right) -\rho \boldsymbol{g}\left(\beta_{\mathrm{T}}\left(T-T_0\right)+\beta_{\mathrm{C}}\left(C-C_0\right)\right) +(1-P)\boldsymbol{S}_{\mathrm{Slurry}}+P\boldsymbol{S}_{\mathrm{rigid}} \tag{1}$$

$$\frac{\partial \rho}{\partial t}\ \nabla\cdot(\rho \boldsymbol{u})=0 \tag{2}$$

$$\frac{\partial(\rho h)}{\partial t}+\nabla\cdot(\rho \boldsymbol{u}h)=\nabla\cdot\left(\frac{k}{c_{\mathrm{ps}}}\nabla h\right) +\nabla\cdot\left(\frac{k}{c_{\mathrm{ps}}}\nabla\left(h_{\mathrm{s}}-h\right)\right)-\nabla\cdot\left(\rho\left(\boldsymbol{u}-\boldsymbol{u}_{\mathrm{s}}\right)\left(h_{\mathrm{l}}-h\right)\right) \tag{3}$$

$$\frac{\partial(\rho C)}{\partial t}+\nabla\cdot(\rho \boldsymbol{u} C)=\nabla\cdot\left(\alpha_l\rho_l D_l\nabla C\right)$$
$$+\nabla\cdot\left(\alpha_l\rho_l D_l\nabla(C_l-C)\right)-\nabla\cdot\left(\rho(\boldsymbol{u}-\boldsymbol{u}_s)(C_l-C)\right) \quad (4)$$

where ρ is the density, $\boldsymbol{u}$ is the flow velocity, t is the time, p is the pressure, μ is the viscosity, g is the gravitational acceleration, β_T is the volume thermal expansion coefficient, β_C is the volume solutal expansion coefficient, T_0 is the reference temperature, C_0 is the reference composition, P is the packing variable, $\boldsymbol{S}_{Slurry}$ is the source term for mushy zones, $\boldsymbol{S}_{rigid}$ is the source term for solid zones, h is the enthalpy, k is the thermal conductivity, c_p is the heat capacity of solid, C is the composition, α is the volume fraction, D is the diffusion coefficient, the subscripts s and l indicate the solid and liquid phases, respectively.

The model used of the slurry and solid parts was that proposed by Plotkowski and Krane[5] and Coleman and Krane[6]. The packing variable, P, can be written as

$$P=\min\left(\max\left(\left(1-\frac{\alpha_s^c-\alpha_s}{\Delta\alpha_s}\right),0\right),1\right) \quad (5)$$

α_s^c is the critical solid fraction at the flow-arrest limit, and $\Delta\alpha_s$ is the steepness of phase transition. If α_s is greater than 0 and less than α_s^c, then P is 0. If α_s is greater than α_s^c and less than 1, then P is 1.

The source term for mushy and solid zones can be written by

$$\boldsymbol{S}_{Slurry}=-\nabla\cdot\left(\mu_l\frac{\rho f_s}{\rho_l}\nabla\boldsymbol{u}_s\right)+\nabla\cdot\left(\overline{\mu_s}\left(1-\alpha\right)\nabla\boldsymbol{u}_s\right)$$
$$-\nabla\cdot\left[\left(\frac{\rho f_s}{\rho_l}\right)(\boldsymbol{u}-\boldsymbol{u}_s)(\boldsymbol{u}-\boldsymbol{u}_s)\right] \quad (6)$$

$$\boldsymbol{S}_{rigid}=-\frac{\mu_l}{K}\frac{\rho}{\rho_l}(\boldsymbol{u}-\boldsymbol{u}_s) \quad (7)$$

where $\overline{\mu_s}$ is the effective solid viscosity, f is the mass fraction, and K is the permeability, which is described by the following Blake–Kozeny model[7].

The solid velocity $\boldsymbol{u}_s$ is modeled as

Table 1 Physical properties and operating parameters for numerical simulation.

Parameters	Marks	Values	Unit
Density of Melt	ρ_l	2350	kg/m^3
Density of Solid	ρ_s	2650	kg/m^3
Heat Capacity of Melt	c_{pl}	1180	J/kg・K
Heat Capacity of Solid	c_{ps}	1000	J/kg・K
Thermal Conductivity of Solid	k_s	140	W/m・K
Kinematic Viscosity	v	5.47×10^{-7}	m^2/s
Thermal Expansion Coefficient	β_T	6.90×10^{5}	1/K
Solutal Expansion Coefficient	β_C	3.20×10^{-1}	–
Eutectic Temperature	T_e	723	K
Eutectic Concentration	C_e	0.38	–
Partition Coefficient	k_p	0.47	–
Latent Heat	L	389000	J/kg
Gravitational Acceleration	g	9.81	m/s^2
Critical Solid Volume Fraction	α_s^c	0.30	–
Smooth Parameter of Packing Fraction	$\Delta\alpha_s$	0.05	–
Secondary Dendrite Arm Spacing	λ	5.00×10^{-5}	m
Diameter of Floating Particle	d_g	7.50×10^{-5}	m
Averaged Solid Viscosity	$\overline{\mu_s}$	6.45×10^{-3}	Pa・s
Casting Speed	$\boldsymbol{u}_{cast}$	50, 70, 90	mm/min

Table 2 Calculation conditions.

	Casting Speed (mm/min)	Distributor model
Calculation #1	50	(A)
Calculation #2	70	(A)
Calculation #3	90	(A)
Calculation #A	70	(A)
Calculation #B	70	(B)
Calculation #C	70	(C)

Table 3 Size of each distributor.

Marks	Metal inlet (Φ mm)	Width × Thickness × Depth (mm)
(A)	60	275 × 105 × 30
(B)	60	105 × 105 × 20
(C)	30	105 × 105 × 20

$$\boldsymbol{u}_s = (1-P)\left(\boldsymbol{u} + f_l\left(\frac{\alpha(\rho_s-\rho_l)d_g^2}{18\mu_l}\,g\right)\right) + P\boldsymbol{u}_{cast} \tag{8}$$

where d_g is the diameter of floating solid particle, and $\boldsymbol{u}_{cast}$ is the casting velocity.

The physical properties and operating parameters are shown in **Table 1**. In this numerical simulation, Al-5.0mass%Mg alloy was used to simplify the numerical simulation model. **Table 2** shows the calculation conditions.

This study focused on the influence of distributor geometry and casting speed on the formation of channel-type segregation. The effect of casting speed was evaluated in calculations #1–#3, and the influence of the distributor was assessed in calculations #A–#C. **Fig. 4** shows the schematic view of the distributors, calculation domain, and boundary conditions. To evaluate the influence of melt distribution, three different distributor models were devised. Distributor model (A) is the default distributor model that supply molten metal to the width direction of slab. The geometry of distributor in model (B) and (C) is square and supply molten metal to width, thickness, and depth directions. Distributor model (C) has a smaller diameter inlet into which molten metal inflows than the other models. The sizes of each distributor model are shown in **Table 3**.

As for the boundary conditions, in all distributor models, the distributor surface through which the molten metal passes was set to occur a pressure drop based on the Darcy law. Primary cooling and heat extraction from the bottom block were calculated based on Newton's cooling law, and both using a constant heat transfer coefficient. Secondary cooling with coolant was also calculated based on Newton's cooling law, and the heat transfer coefficient was set so that the value depends on the surface temperature of slab. **Fig. 5** (a) shows the numerical grid. The slab size was 400 mm × 800 mm, to reduce the calculation time the calculation domain was limited to a quarter-

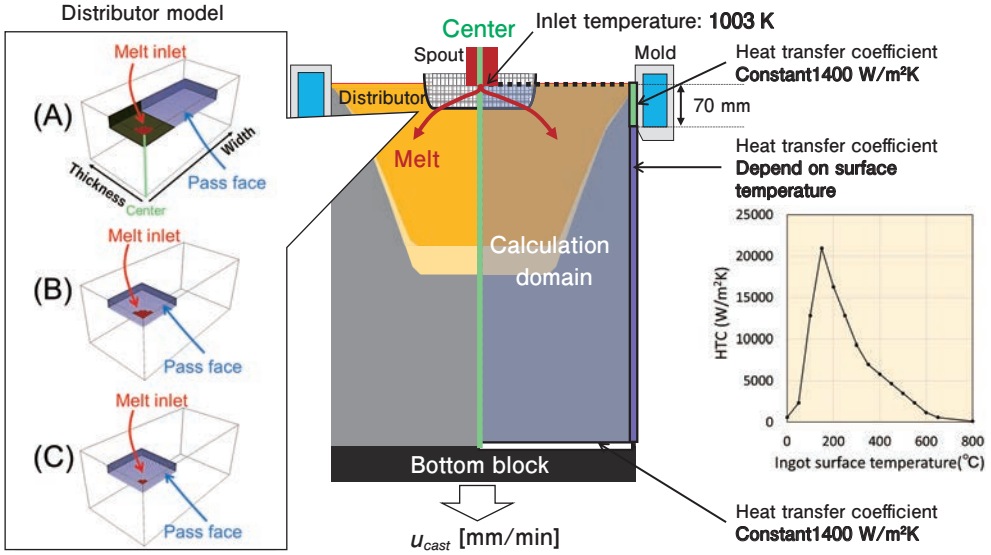

Fig. 4 Schematic view of the distributors, calculation domain, and boundary conditions.

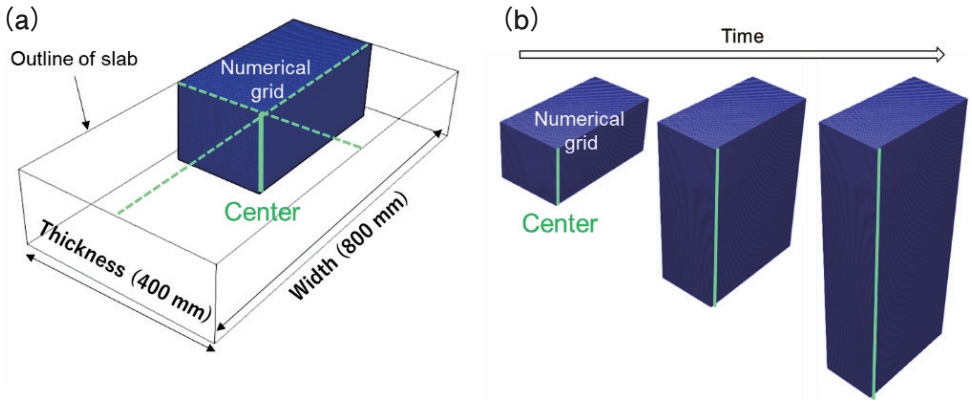

Fig. 5 Schematic view of (a) numerical grid and (b) dynamic grid motion.

symmetrical region of the slab. While finer mesh resolutions typically enhance the fidelity of flow calculations, the grid cell size was uniformly set to 5 mm in all directions to alleviate the computational load. Fig. 5 (b) shows schematic drawing of dynamic grid motion. In DC casting, typical casting length of produced slabs is several meters, so in the present study, the dynamic grid motion was implemented by adding new grid cells.

All the above numerical models were incorporated into an open-source software, OpenFOAM (v1812).

3. Results and Discussion

Fig. 6 shows the numerical simulation result of time variation in temperature and Mg concentration distribution within a slab at calculation #2. It can be seen that stripe-shaped negative segregation is formed successively along the solidification front in the thickness section as casting proceeds. **Fig. 7** and **Fig. 8** show the results of Mg concentration distribution within a slab for the same casting length, and the graph plots the normalized Mg concentration by the average concentration in the thickness section of each slab. In Fig. 7, it is compared the difference of Mg concentration distribution each casting speed. As far as the standard deviation of Mg concentration is concerned, the casting speed and channel-type segregation strength is tiny correlations, and it is not expected to suppress the segregation by controlling casting speed.

In Fig. 8, the differences in Mg concentrations distribution for each distributor model are compared. The result of calculation #B has a smaller segregation

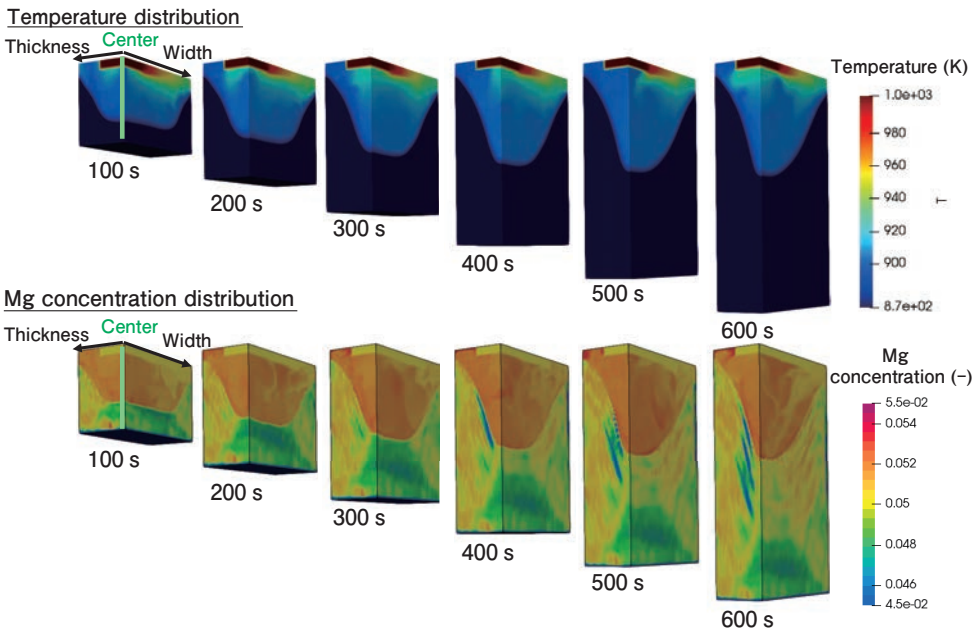

Fig. 6 Time variation in temperature and Mg concentration at calculation#2.

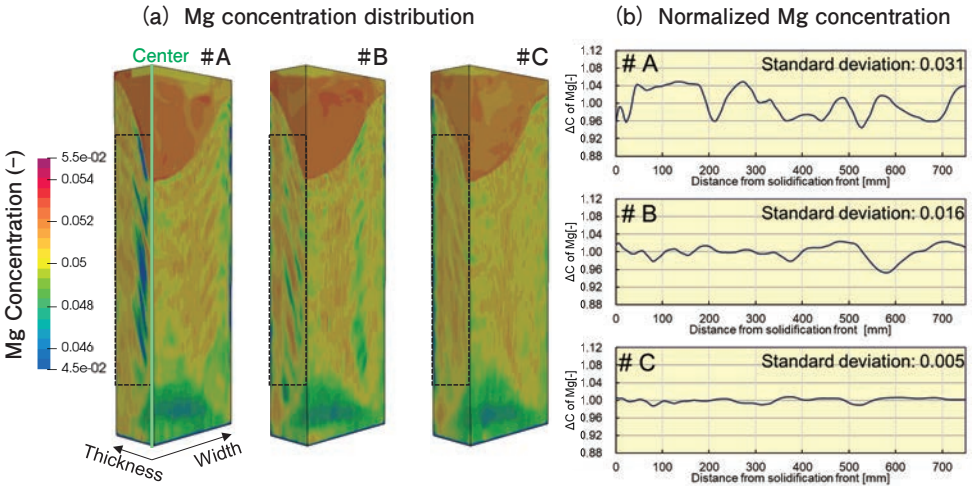

Fig. 7 (a) Mg concentration distribution within a slab at each casting speed, and (b) the graphs of the normalized Mg concentration by the average concentration in the thickness section of each slab.

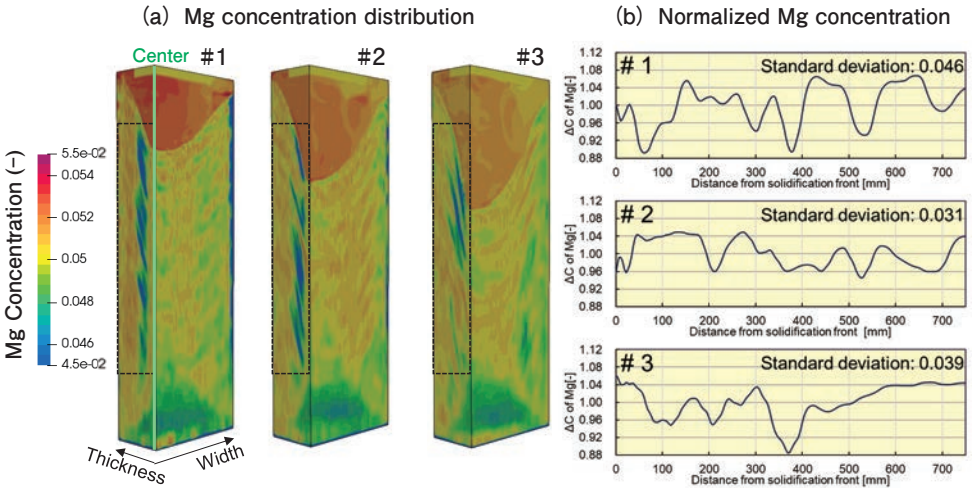

Fig. 8 (a) Mg concentration distribution within a slab at each distributor model, and (b) the graphs of the normalized Mg concentration by the average concentration in the thickness section of each slab.

concentration than calculation #A, but the segregation appears in a width cross section too. The result of calculation #C has an even smaller segregation concentration than calculation #B, and the segregation is suppressed in both the width and thickness cross sections.

Fig. 9 shows the concentration distribution of Mg and flow fields in the molten sump. At calculation #A, it can be seen that the molten metal forms circular flow that flows from distributor to width direction of slab, next flows downward along the solidification front to center of slab, finally flows upward along the solidification front to thickness direction of slab. This circular flow allows molten metal to flow in the same direction as the upward solutal buoyancy flow at the solidification front in thickness direction. Therefore, the high Mg concentration zone is widely distributed at the solidification front, and the partitioning of solute is promoted, resulting in pronouncing the channel-type segregation in thickness cross section.

At calculation #B, molten metal flows in both the thickness and width directions, so circular flow as # A does not occur, but it can be seen that the downward flow separate at bottom of molten sump and exerts an upward flow in both the thickness and width direction. As a result, it is considered the high Mg concentration zone occur and the channel-type segregation was formed in both thickness and width cross section.

At calculation #C, inlet size is smaller than the other models, resulting in a higher inflow velocity.

As a result, circular flow does not occur and downward flow against upward solutal buoyancy flow occurs throughout molten sump. Therefore, it is

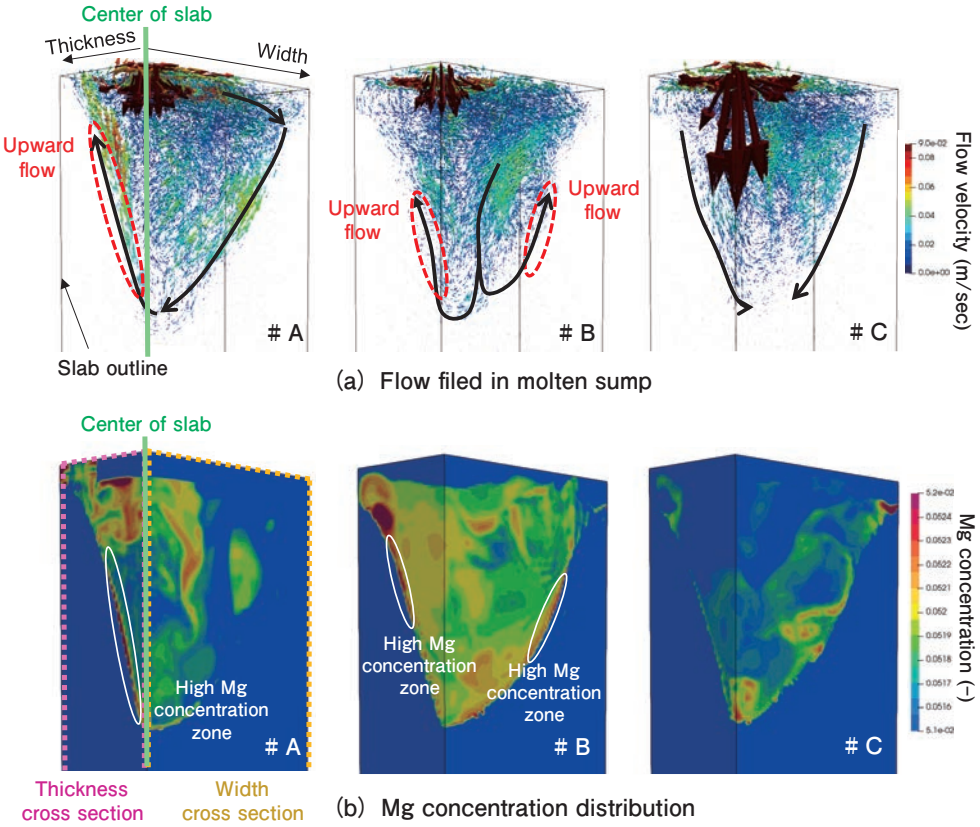

Fig. 9 (a) Flow field in molten sump and (b) Mg concentration distribution.

considered that the solute was diffuse in molten sump without collecting at the solidification front and the channel-type segregation did not occur in both thickness and width cross section.

4. Conclusion

In this study, channel-type segregation in DC casting of aluminum slabs was reproduced by numerical analysis, and the following results were obtained.

1. Channel-type segregation occurs at different locations in slab depending on the geometry of distributor.
2. Channel-type segregation is more pronounced in the high Mg zone formed by the molten metal upward flow at solidification front.
3. By reducing the area of molten metal inlet, the molten metal inflow velocity increase and strong downward flow occur throughout molten sump. Therefore, Mg concentration at the solidification front is suppressed and channel-type segregation can be reduced.

REFERENCES

1) T. Yamamoto, K. Kamiya, K. Fukawa, S. Yomogida, T. Kubo, M. Tsunekawa and S. Komarov: Metall. Mater. Trans. B, **52** (2021), 4046-4060.
2) Y.F. Cao, Y Chen, D.Z. Li, H.W. Liu and P.X.Fu.: Metall. Mater. Trans. A, **47** (2016), 2927-2939.
3) C.J. Vreeman, M.J.M. Krane and F.P. Incropera: Int. J. Heat Mass Transf., **43** (2000), 677-686. (2000)
4) K. Fezi, A. Plotkowski and M.J.M. Krane: Numer. Heat Transf. A, **70** (2016), 939-963.
5) A. Plotkowski and M.J.M. Krane: Mater. Sci. **124** (2016), 238-248.
6) J. Coleman and M.J.M Krane: Mater. Sci. Technol **36** (2020), 393-402.
7) D. M. Stefanescu: Science and engineering of casting solidification, (2008), Springer, New York.

Keisuke Kamiya
Process Research Department,
Research & Development Center,
Marketing & Technology Division,
UACJ Corporation.

Takuya Yamamoto
Osaka Metropolitan University,
Department of Chemical Engineering,
Associate Professor, Ph.D. (Eng.)